Nanoscopic Poly(ethylene oxide) Strands Embedded in Semi-Interpenetrating Methacrylate Networks. Preparation Method and Quantitative Characterization by Field-Gradient NMR Diffusometry

Elmar Fischer,*,† Uwe Beginn,‡ Nail Fatkullin,§ and Rainer Kimmich†

Sektion Kernresonanzspektroskopie, Universität Ulm, Albert-Einstein-Allee 11, D-89069 Ulm, Germany, DWI/ITMC/TexMC, RWTH-Aachen, Worringerweg 1, D-52056 Aachen, Germany, and Department of Physics, Kazan State University, Kazan 420008, Tatarstan, Russia

Received December 3, 2003; Revised Manuscript Received February 4, 2004

ABSTRACT: Networks of nanoscopic strands of linear, monodisperse poly(ethylene oxide) embedded in cross-linked methacrylate matrices were prepared. Depending on the choice of matrix constituents, the diameters of these strands can be varied considerably. The samples were characterized by DSC, TEM, SEM, and fringe field gradient NMR diffusometry with respect to the strand diameter. A formalism evaluating diffusive spin−echo attenuation curves based on the tube/reptation model is presented permitting the determination of the tube diameter. Values in the range from 8 to 58 nm were found in accordance with TEM micrographs of shadow-cast freeze-fractured surfaces of the samples.

Introduction

The semi-interpenetrating networks (semi-IPNs) considered in this study consist of a cross-linked methacrylate matrix of varying composition and an interlaced network of strands of linear poly(ethylene oxide) (PEO). The motivation to study this sort of system is 3-fold. First, it is of major interest to develop preparation techniques for semi-IPNs with well-defined embedded polymer nanostrands. Second, this is an example demonstrating that field gradient NMR diffusometry can be utilized to determine the width of such polymer strands nondestructively. A corresponding experimental protocol and a suitable evaluation formalism are reported. Third, this sort of system permits one to study chain dynamics in polymer melts confined to a nanoporous quasi-solid matrix. Any confinement effects are considered to have a strong impact on our understanding of polymer dynamics in general.

The first problem to be solved in studies of translational diffusion of long macromolecules in narrow pores is the preparation of solid nanoporous systems completely filled with mobile linear polymers. Instead of trying to fill a given porous medium according to the so-called bulk-to-bulk method, which often requires excessively long preparation times or results in bad filling degrees, we prepared semi-interpenetrating networks:[1−3] Empty "pores" never occur in this protocol, but are prepared already filled with linear polymers in the form of nanoscopic strands dispersed in the matrix consisting of another polymer species strongly cross-linked and consequently immobilized. The experiments are then carried out at a temperature where the embedded polymer strands are molten while the cross-linked matrix remains in a quasi-solid state.

In the following, the terms (polymer filled) "pore" or "pore channel" and polymer "strand" (embedded in a matrix) will be used synonymously, whereas the expression "tube" is selectively used in the sense of the tube/reptation model for polymer dynamics.[4] Actually it will be shown that the "pores" referred to in the present NMR diffusometry study act as "tubes" in this sense. However, this is a question of the time scale: On much shorter time scales as they are relevant for NMR relaxometry it was shown elsewhere[5] that much smaller "tube" diameters are effective. The term "tube" is related to polymer dynamics, whereas "pore" or "embedded strand" is considered to be a micro- or nanostructural feature imposing some topological constraint on polymer diffusion.

Preparation Technique for Semi-Interpenetrating Networks

The semi-interpenetrating networks investigated here consist of a cross-linked methacrylate matrix of varying composition and an interlaced network of strands of linear poly(ethylene oxide) (PEO). The weight-average molecular mass of the PEO is $M_w = 10\,170$ g/mol (polydispersity $M_w/M_n \approx 1.07$), which is well above the critical molecular weight. The basic principles of the preparation technique were described in a previous paper:[6] Solutions of PEO in 2-hydroxyethyl methacrylate (HEMA)/1,2-ethanediol dimethacrylate (EGDMA) mixtures were rapidly quenched into the instable regions of their phase diagrams. During the cooling process, spinodal decomposition occurred causing the formation of networks of interconnected "wormlike" structures of the separated gel phase. These transient structures were conserved by vitrification in the course of further cooling below the glass transition temperature of the mixtures. The glasses were then carefully heated above their glass temperature, leading to rapid crystallization of the PEO within the polymer-enriched regions combined with the radial collapse of those "worms" to form the strands of interest. This peculiar microphase segregated bulk morphology can be fixed permanently by subsequent UV-induced free radical polymerization and cross-linkage of the methacrylate solvent.[6]

According to the Cahn−Hilliard−van Aartsen theory of spinodal demixing in polymer solutions,[7,8] the initial diameter of the strands consisting of the polymer-rich phase obeys[7]

$$d_m \propto \left(1 - \frac{T_Q}{T_S}\right)^{-1/2} \quad (1)$$

* Corresponding author. E-mail: elmar.fischer@physik.uni-ulm.de.
† Universität Ulm.
‡ RWTH-Aachen.
§ Kazan State University.

10.1021/ma0358226 CCC: $27.50
Published on Web 04/08/2004

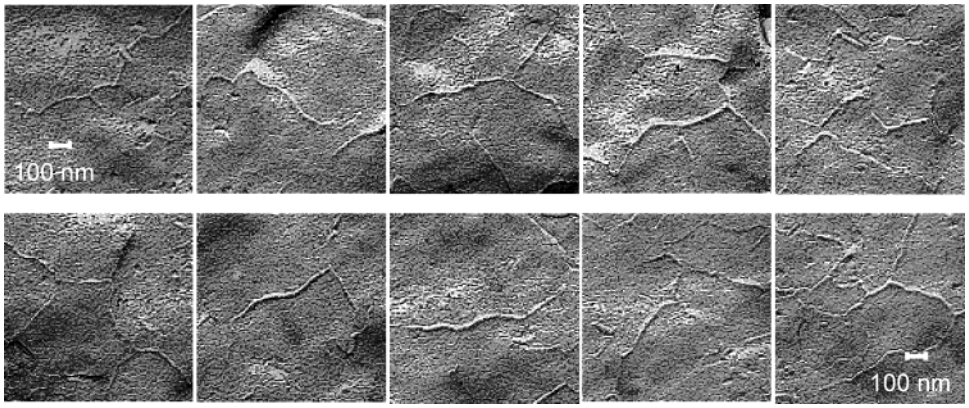

Figure 1. Typical electron micrographs of PEO strands in a quasi-solid methacrylate matrix.[6] The strand diameter is about 10 nm.

where T_Q is the quenching temperature of the solution and T_S is the spinodal demixing temperature of the polymer solution. Typical strand diameters found in ref 6 were about 10 nm. Equation 1 offers two orthogonal approaches to prepare considerably larger diameters: (i) the "thermal treatment" approach by changing T_Q, and (ii) the "solubility approach" by varying the temperature T_S. Since quenching is performed by bringing the material in contact to a metal block precooled to T_Q, approach i is straightforward. On the other hand, the demixing temperature T_S will depend on polymer concentration and the chemical nature of the solvent and can hence be controlled by using different monomer mixtures as solvents. Note that crystallization of the polymer must not occur before the majority of the polymer is segregated into the gel phase, since "free" crystallization in the sol phase would generate lamellar crystals instead of the desired strandlike solid structures. The separation of the glass temperature of the polymer solution relative to the demixing and crystallization temperature is of paramount importance for the success of the sample preparation. It turned out that it can be controlled most efficiently by using monomer solvents other than the HEMA/EGDMA system.

In the present study, the following materials were employed: poly(ethylene oxide)s (PEO-10000, $M_w = 10\ 170$ g/mol, $M_w/M_n \approx 1.07$; (Aldrich); PEO-11200, $M_w = 11\ 200$ g/mol, $M_w/M_n = 1.04$ (Polymer Standards) and benzoine monomethyl ether (Röhm). These substances were used as received. Methyl acrylate (Röhm), methyl methacrylate (Aldrich), 2-hydroxyethyl methacrylate (HEMA) (Fluka), *n*-dodecyl methacrylate (DMA) (Fluka), *n*-hexyl methacrylate (Röhm), ethylene glycol dimethacrylate (EGDMA) (Fluka), and *n*-hexanediol dimethacrylate (HDDMA) (Aldrich) were distilled in vacuo over calcium hydride prior to use.

The semi-interpenetrating networks were prepared as follows. Monomer, cross-linker, and benzoine monomethyl ether (photoinitiator) were weighed (ratio 80:20:0.5 by weight) into 10 mL round-bottomed flasks. Polymer solutions were prepared shortly before use by weighing the poly(ethylene oxide) (accuracy ±0.005 mg) into 1.5 mL screw cap vials (LabTop) and adding the monomer/cross-linker/photoinitiator mixture. The closed glasses were heated cautiously until a clear solution was obtained. For polymerization the solutions were degassed at ambient temperature by repeated freeze−thawing cycles.

Quenching and photopolymerization were performed in nitrogen atmosphere in a glovebox. Polyethylene molds with lids (o.d. = 25 mm, CibaVision) were inserted into an aluminum block[6] and precooled to the corresponding quenching temperature. Using a preheated syringe, 150−200 μL of an isotropic solution of PEO in the methacrylate monomers was injected rapidly into the cold mold. Subsequently, the lid was placed on the liquid drop and pressed down strongly for 1 min. After heating to the selected polymerization temperature, the samples were irradiated through polyethylene lids using two 366 nm, 4 W UV lamps for more than 16 h. Finally, the samples were postcured at room temperature for 24−36 h using a standard 366 nm/15 W UV laboratory lamp.

Sample Characterization Methods

All samples were characterized with differential scanning calorimetry (DSC) in order to determine the melting transitions of the embedded crystalline PEO fractions. Since the melting temperatures of small crystallites depend on crystal size,[9] DSC is a method for rough estimations of the PEO strand diameters. The instrument was a Perkin-Elmer DSC 7 unit, calibrated against indium and ultrapure water standards. Gel samples (typical weight: 20 mg) were sealed tightly into Perkin-Elmer pressure pans and quenched in liquid nitrogen just before the measurement. Polymerized samples (typical weight: 5 mg) were enclosed in standard Perkin-Elmer 30 μL/0.15 aluminum pans. In all cases a heating rate of 10 K/min was chosen.

To visualize the nanostructure of the samples, transmission electron micrographs (TEM) were recorded with a Phillips EM301 microscope operated at 80 kV. Attempts to prepare ultrathin sections of the material failed. Therefore, the freeze-fraction/replication technique was applied. The samples were immersed into liquid nitrogen and fractured at −180 °C. In a Balzers BF freeze etching chamber, the surfaces were coated in vacuo with a 2.5 nm platinum layer under an angle of 37°. The metal layer was reinforced by deposition of a 25 nm carbon film. The replica was removed from the sample surface by flotation in an aqueous 10 wt % KOH solution for 3 days. Typical electron micrographs of the resulting PEO strands in the methacrylate matrix are shown in Figure 1.

Field-emission scanning electron microscopy (FE-SEM) was performed with a HITACHI S 5200 instrument. The samples were cooled to −150 °C in a Balzers BF freeze etching chamber and fractured at that temperature. Surfaces were rotary shadowed in vacuo with a 2 nm platinum layer. In contrast to TEM investigations, the metal film on the surface can be investigated directly. No reinforcement of the metal film is necessary.

Determination Method for the PEO Strand Diameter with the Aid of NMR Diffusometry

The principal method with which the semi-interpenetrating network samples were investigated in this study was steady field gradient NMR diffusometry[10] in the fringe field of a 9.4 T Bruker wide-bore magnet. The fringe-field gradient at the measuring position was $G = 60$ T/m at a proton resonance frequency of $\nu = 200$ MHz. The usual stimulated echo pulse sequence

$$\frac{\pi}{2} - \tau_1 - \frac{\pi}{2} - \tau_2 - \frac{\pi}{2} - \text{echo}$$

was employed, varying the time τ_1 and keeping τ_2 at a constant value for a chosen diffusion time $t_D \simeq \tau_2$, $\tau_2 \gg \tau_1$.

Table 1. Effects of the PEO Concentration and the Thermal Treatment of Polymer Solutions on the Melting Temperatures of Embedded PEO Crystals (PEO-10000, HEMA:EGDMA = 8:2 w:w, 0.5 wt % Photoinitiator)[a]

id.	μ(PEO) [wt %]	T_Q [K]	T_P [K]	peak 1 $\vartheta_{ons}^{(1)}$ [°C] ($\Delta H_m^{(1)}$ [J g^{-1}])	peak 2 $\vartheta_{ons}^{(2)}$ [°C] ($\Delta H_m^{(2)}$ [J g^{-1}])	$\Delta H_m^{(1)}$:$\Delta H_m^{(2)}$ [%:%]	$\Sigma\Delta H_m^{(i)}$ [J/g] (Q [%])
1	20	273	273	40.0 (...)	46.0 (n.d.)	n.d.[b]	21.5 (57.4)
2	20	273	223	48.4 (8.4)	56.6 (17.9)	31.9:68.1	26.3 (70.2)
3	20	263	263	43.3 (9.2)	52.2 (14.4)	40.2:59.8	23.6 (63.0)
4	30	253	263	43.1 (14.8)	53.5 (26.7)	35.7:64.3	41.5 (73.8)
5	35	253	263	43.1 (15.6)	53.3 (32.9)	32.2:67.8	48.5 (74.0)
6	40	253	263	42.6 (16.0)	53.3 (38.6)	29.3:70.7	54.0 (72.0)
7	50	253	263	45.0 (n.d.)	53.2 (n.d.)	n.d.[b]	58.8 (62.7)
8	20	253	253	40.4 (11.1)	51.2 (15.4)	41.9:58.1	26.5 (70.7)
9	20	223	223	44.9 (18.1)		100:0	18.1 (48.3)
10	20	153	223	44.6 (21.4)		100:0	21.4 (57.1)
11	20	123	223	37.3 (5.3)		100:0	5.3 (14.4)
12	20	103	223	45.2 (24.0)		100:0	24.0 (64.0)
13	20	93	223	39.5 (26.0)		100:0	26.0 (69.4)

[a] μ(PEO) = content of PEO-10000 in the methacrylate mixture, T_Q = quenching temperature, T_P = polymerization temperature, $\vartheta_{ons}^{(i)}$ = onset temperature of peak i, $\Delta H_m^{(i)}$ = melting enthalpy of peak i, $\Sigma\Delta H_m^{(i)} = \Delta H_m^{(1)} + \Delta H_m^{(2)}$, $Q = 100\% \Sigma\Delta H_m^{(i)}/\{\mu(\text{PEO})\Delta H_m^{(\text{PEO})}\}$, and n.d. = not detected. [b] Peaks not separated.

To improve the signal-to-noise-ratio, the number of accumulated scans was incremented with increasing τ_1 value by a factor of 3 every $8\tau_1$ intervals. Echo attenuation effects other than by translational diffusion, were eliminated in comparative measurements with another 200 MHz instrument with negligible field gradient. Quotients formed of echo amplitudes with and without field gradient thus provide the attenuation curves due to diffusion alone (see also ref 11, where the same experimental protocol was employed). In a recent paper,[12] an alternative method is described without need of a second instrument.

Diffusion in bulk samples of PEO-10000 was investigated separately in order to rule out any polydispersity effects. In this case, no deviations from a Gaussian echo attenuation behavior was observed as expected for unrestricted diffusion in the limit beyond the terminal chain relaxation time. This corroborates the narrow polydispersities of the PEO samples.

The quotient of echo amplitudes with and without gradient was formed and normalized for the shortest τ_1 value where attenuation by diffusion is still negligible. The evaluation formula (see eq 19 in the Appendix) was fitted to the data in logarithmic form so that all data points entered into the least-squares fitting procedure with weights in the same order of magnitude.

The diffusion time $t_d \approx \tau_2$ was kept fixed in each experiment while τ_1 was varied. All NMR experiments were performed at 80 °C. At this temperature, the proton transverse relaxation time T_2 of the P[(HEMA/DMA)$_{0.8}$-*cross*-HDDMA$_{0.2}$] matrix is about 200 μs whereas PEO melts have T_2 values of several milliseconds depending on the pore diameter.[5] Signals from the matrix can thus safely be neglected relative to the PEO signals in our experiments for the τ_1 values examined.

Reptation of polymer chains implies anomalous diffusion characteristics with a non-Gaussian propagator.[4,13] The standard spin echo attenuation formula[10] is therefore not appropriate for evaluations of experimental data when reptation is suspected to be the dominating diffusion mechanism. An evaluation formalism specifically valid for this case was reported in a previous paper.[14] A tight tube was assumed in that treatment, not permitting any perceptible lateral displacements of the entrapped polymer chains. On the other hand, in the current study, the pore diameter is varied in a wide range so that such internal diffusion degrees of freedom may influence attenuation curves. Therefore, a correspondingly modified formalism became necessary and is outlined in the Appendix (see eq 19). On this basis, the pore diameter can be evaluated reliably. The values fitted to the experimental data turned out to be independent of the diffusion time $t_d \approx \tau_2$ within the experimental error of less than 10%. The diameter data given below are values averaged over 10 different τ_2 intervals in each case ranging from 10 to 100 ms.

Results

Different Preparation Conditions in the Light of DSC. To optimize the preparation conditions of the samples with the objective to cover a range of PEO strand diameters as wide as possible, a number of parameters have been varied and characterized with the aid of DSC as a means for crude and quick estimations of the PEO strand diameter resulting under the preparation conditions. The results will be summarized in Tables 1−3. The DSC data in Table 1 demonstrate the effect of different polymerization and quenching temperatures, T_P and T_Q, respectively. The following conditions were concluded for optimal formation of PEO strands: T_P < 223 K and T_Q < 123 K. The second preparation parameter to be examined is the composition of the solvent in which the PEO is dissolved initially. The DSC data in Table 2 for a series of different solvent components demonstrate that the polarity of the molecules play a decisive role for the PEO strand formation. In light of these data, the combination HEMA + DMA in varying compositions turned out to be favorable for the preparation of samples with different PEO strand diameters. The DSC data of the samples studied by NMR diffusometry are summarized in Table 3.

In a first series of experiments, the thermal treatment of semi-IPNs of PEO-10 000 in P[HEMA$_{0.8}$-*cross*-EGDMA$_{0.2}$] was examined with the aid of DSC. The homogeneous solutions were shock frozen ($dT/dt \approx 50-100$ K/s) by bringing them in close contact to polyethylene molds precooled to the "quenching temperature" T_Q (see above). Subsequently, the samples were allowed to thaw slowly ($dT/dt \approx 0.5-0.75$ K/min) to the respective polymerization temperature T_P and were then solidified by UV-light-initiated free radical polymerization and cross-linkage. According to the DSC curves, the cross-linked matrix itself did not show any phase transition in the investigated temperature range.

For the system, PEO/P[HEMA$_{0.8}$-*cross*-EGDMA$_{0.2}$], the following empirical relation between the strand diameter and the onset temperature of the melting endotherm was established:[6]

$$d_s = \frac{263 \text{ nm °C}}{\vartheta_{ons} - \vartheta_0^{PEO}} \qquad (2)$$

Table 2. Effect of Different Methacrylate Solvents on the Melting Temperatures of Embedded PEO (20 wt % PEO-10000, Monomer:EGDMA = 8:2 w:w, 0.5 wt % Photoinitiator)[a]

id	monomer	T_Q [K]	T_P [K]	peak 1 $\vartheta_{ons}^{(1)}$ [°C] ($\Delta H_m^{(1)}$ [J g^{-1}])	peak 2 $\vartheta_{ons}^{(2)}$ [°C] ($\Delta H_m^{(2)}$ [J g^{-1}])	$\Delta H_m^{(1)}$:$\Delta H_m^{(2)}$ [%:%]	$\Sigma\Delta H_m^{(i)}$ [J/g] (Q [%])
14	HEMA	173	223	37.5 (19.3)		100:0	19.3 (51.5)
15	HEA	93	223	35.4 (27.9)		100:0	27.9 (74.5)
16	HPMA	173	223	42.7 (22.2)		100: 0	22.2 (59.3)
17	GMA	173	223	41.7 (n.d.)	47 (n.d.)	n.d.[b,c]	28.7 (76.6)
18	FMA	173	223	41.7 (21.8)		100:0	21.8 (58.2)
19	MMA	173	223	38.4 (13.9)	46.0 (7.5)	65.0:35.0	21.4 (57.1)
20	EMA	173	223	38.2 (8.5)	49.3 (16.9)	33.5:66.5	25.4 (67.8)
21	*t*-BMA	173	223	47.1 (n.d.)	53.4 (n.d.)	n.d.[b]	31.5 (84.0)

[a] μ(PEO) = PEO-10.000 content in methacrylate mixture, T_Q = quenching temperature, T_P = polymerization temperature, $\vartheta_{ons}^{(i)}$ = onset temperature of peak i, $\Delta H_m^{(i)}$ = melting enthalpy of peak i, $\Sigma\Delta H_m^{(i)} = \Delta H_m^{(1)} + \Delta H_m^{(2)}$, Q = 100% $\Sigma\Delta H_m^{(i)}/\{\mu(\text{PEO})\Delta H_m^{(\text{PEO})}\}$, HEMA = 2-hydroxyethyl methacrylate, HEA = 2-hydroxyethyl acrylate, HPMA = 3-hydroxypropyl methacrylate, GMA = 2-glycidylpropyl methacrylate, FMA = furfuryl methacrylate, MMA = methyl methacrylate, EMA = ethyl methacrylate, *t*-BMA = *tert*-butyl methacrylate, and n.d. = not detected. [b] Peaks not separated. [c] Very broad signal.

Table 3. DSC Characterization of the Samples Studied by NMR Diffusometry: Effects of the Methacrylate Composition of HEMA/DMA/HDDMA Mixtures on the Melting Temperatures of Embedded PEO Crystals (20 wt % PEO-10000, 16 wt % HDDMA, 0.5 wt % Photoinitiator, T_Q = 93 K, T_P = 223 K)[a]

	HEMA: DMA					
id	concn [wt %:wt %]	ratio [%:%]	peak 1 $\vartheta_{ons}^{(1)}$ [°C] ($\Delta H_m^{(1)}$ [J g^{-1}])	peak 2 $\vartheta_{ons}^{(2)}$ [°C] ($\Delta H_m^{(2)}$ [J g^{-1}])	$\Delta H_m^{(1)}$:$\Delta H_m^{(2)}$ [%:%]	$\Sigma\Delta H_m^{(i)}$ [J/g] (Q [%])
22	63.2:0.0	100:0	39.8 (21.5)		100:0	21.5 (56.9)
23	57.2:6.4	90:10	46.9 (27.2)		100:0	27.2 (72.0)
24	56.8:6.3	90:10	32.8 (24.4)	n.d.[b,c]		24.4 (64.6)
25	50.8:12.6	80:20	41.1 (26.6)	n.d.[b,c]		26.6 (70.4)
26	41.5:21.8	66:34	37.5 (12.9)	≈46.9 (12.3)[b]	51.2:48.8[b]	25.2 (66.7)
27	36.5:26.3	58:42	40.6 (12.9)	≈49.2 (12.7)[b]	50.4:49.6[b]	25.6 (67.7)
28	33.3:30.9	52:48	39.0 (23.2)	n.d.[b,c]		23.2 (61.4)
29	31.8:31.7	50:50	39.1 (27.9)	≈48.5 (...)[b,c]		27.9 (73.8)
30	28.6:34.9	45:55	38.8 (23.2)		100:0	23.2 (61.4)
31	26.2:37.6	41:59	39.5 (19.3)		100:0	19.3 (51.1)
32	25.4:38.0	40:60	≈34 (...)[b,c]	45.3 (37.8)		37.8 (≈100)
33	25,2:38.1	40:60	38.7 (15.3)		100:0	15.3 (40.5)

[a] $\vartheta_{ons}^{(i)}$ = onset temperature of peak i, ΔH_m^i = melting enthalpy of peak i, $\Sigma\Delta H_m^{(i)} = \Delta H_m^{(1)} + \Delta H_m^{(2)}$, Q = 100% × $\Delta H_m^{(i)}$. HEMA = 2-hydroxyethyl methacrylate, DMA = *n*-dodecyl methacrylate, HDDMA = 1,6-hexanediol dimethacrylate, EGDMA = 1,2-ethanediol dimethacrylate. [b] Signals not separated, $\Delta H_m^{(i)}$ estimated [c] Broad signal.

(d_s = diameter of the embedded PEO strands, ϑ_{ons} = onset temperature of the PEO melting endotherm, in °C, ϑ_0^{PEO} = 62.5 °C). The DSC results for samples with different amounts of PEO, T_Q and T_P, are summarized in Table 1.

Depending on the preparative conditions, either a single or a double peak was obtained. Representative endotherms are shown in Figure 2. Samples that exhibited a single PEO melting endotherm at the first heating cycle, indicative for a monomodal crystal size distribution, were only obtained upon quenching the solutions to temperatures below 153 K *and* initiating polymerization below 223 K (cf. Table 1, entries 10−13). In these cases, the measured melting enthalpy was in the range 21−26 J/g, which is 61−69% of the maximum melting enthalpy that can theoretically be expected if all PEO in the samples would completely crystallize.

The melting temperatures of the PEO crystals in these samples were between 37 and 45 °C, indicating the presence of uniform PEO strands with diameters of around 10.5−15.0 nm.[6] Repeated cooling/heating cycles did not lead to (re-) crystallization signals in such samples. This behavior was attributed to the strong steric confinement of the macromolecules within the fine strands that prevents crystallization.[6]

Quenching to temperatures above 213 K *or* polymerization above 243−253 K resulted in samples that exhibited two melting endotherms in the DSC thermograms (Table 1, 1−8). Curve c in Figure 2 shows a representative DSC thermogram of PEO/P[HEMA$_{0.8}$-*cross*-EGDMA$_{0.2}$] (20 wt % PEO-10 000, HEMA: EGDMA = 8:2 wt: wt, 0.5 wt % photoinitiator) quenched to T_Q = 273 K and polymerized at T_P = 223 K (sample 2 in Table 1).

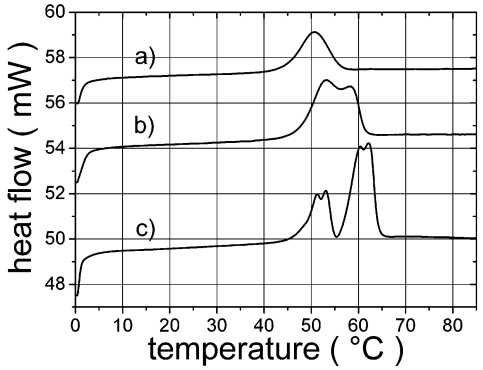

Figure 2. Typical DSC curves of semi-IPNs of 20 wt % PEO-10 000 in P[HEMA $_{0.8}$-*cross*-EGDMA$_{0.2}$] obtained for different quenching and/or polymerization temperature: (a) sample 10, single peak; (b) sample 7, weakly separated double peak; (c) sample 2, well separated double peak.

At constant PEO content of the solutions, the total melting enthalpy of these samples mainly depended on

the applied polymerization temperature. A slight increase was observed with higher temperatures (20 wt % PEO-10000: $T_P = 223$ K, $\Delta H_m^{(i)} = 24-26$ J/g; $T_P = 263$ K, $\Delta H_m^{(i)} = 28$ J/g). When the PEO content was increased at constant preparation conditions (e.g., $T_Q = 253$ K, $T_P = 263$ K, samples 4−7 in Table 1), the total melting enthalpy grew, but the enthalpy yield became lower (for 20 wt % PEO-10000, 78%; for 50 wt % PEO-10000, 63%).

The relative intensity of the peaks showed little variations. The low-temperature peak contributed between 30% and 40% of the total melting enthalpy. Onset temperatures of the low-temperature peak (40−43 °C) indicate the presence of PEO strands and suggest diameters in the range 11.7−13.5 nm according to eq 2. The high-temperature peaks, on the other hand, are attributed to PEO lamellar crystals as could be concluded from scanning electron microscopy investigations.

When performing heating/cooling cycles on these samples, the high-temperature peak was observed reversibly, whereas the low-temperature peak only appeared in the first heating run. Obviously, the embedded PEO crystals leading to the high-temperature DSC peak were large enough not to be affected by confinement with respect to crystallization. Under "intermediate" preparation conditions ($T_Q = 233-243$ K, $T_P = 243-273$ K), the occurrence of two endothermic peaks was erratic and could not be controlled.

In a second screening series, the preparation method was changed. After quenching the solutions, the samples were rapidly heated ($dT/dt \approx 2.5$ K/min) from the quenching to the polymerization temperature and annealed at T_P starting from 2 min up to 6 h. However, no distinct deviations from the detailed results described previously could be detected.

Obviously, the unconfined solution crystallization of PEO-10 000 could only be impeded by "harsh" quenching/polymerizing conditions. Only under theses circumstances are thin PEO strands formed. Reducing the quenching rate and the quenching and the polymerization temperatures, solution crystallization always interfered with the confinement of PEO. No experimental procedure was found that yielded thick PEO strands without any presence of PEO platelet crystals. Consequently, the "thermal control" approach was no longer pursued. Instead, effects of PEO phase separation in a variety of different methacrylate solvents were investigated in more detail.

In the framework of the "solubility approach", it was attempted to tailor the phase separation properties of PEO solutions by changing the methacrylate solvent with the objective to "tune" the polymer solubility. Table 2 summarizes results of screening experiments on methacrylate monomers of various polarity. Note that eq 2 cannot be applied to these samples. However, the DSC analysis is still useful to distinguish mono- and multimodal PEO crystallite size distributions.

Upon quenching to $T_Q = 173$ K and polymerizing at $T_P = 223$ K, samples with polar monomers, e.g., HEMA, 2-hydroxyethyl acrylate (HEA), 3-hydroxypropyl methacrylate (HPMA) and furfuryl methacrylate (FMA), exhibited only a single PEO melting peak in the temperature region between 37 and 42 °C. Less polar or nonpolar monomers like glycidyl methacrylate (GMA), methyl methacrylate (MMA), ethyl methacrylate (EMA) and *tert*-butyl methacrylate (*t*-BMA) yielded DSC thermograms with two endothermic peaks. The temperature ranges of the signal onset temperatures was comparable to that observed with the "thermal control" experiments (compare Tables 1 and 2). Changing the quenching temperature to $T_Q = 223$ K, the quality of the sample deteriorated considerably. Bimodal size distributions were then found also for PEO/HPMA/EGDMA.

On the basis of these experiments, only minor variations in the solution polarity induced strong changes in solubility and phase segregation properties of the PEO/methacrylate mixtures. Hence, samples with a modified matrix consisting of the more polar HEMA and a less polar monomer were investigated.

A possible influence of the cross-linker polarity on semi-IPNs could be ruled out from experiments on mixtures of 20 wt % PEO-10000, 64 wt % HEMA, and 16 wt % cross-linker, in which the cross-linker component ethylene glycol dimethacrylate (EGDMA) partially was replaced by the less polar *n*-hexanediol dimethacrylate (HDDMA). These screening experiments with only a very small change of solvent composition, did not show deviations from previous results, only the melting enthalpy yield was lowered to 60 wt % for the cross-linker mixtures. Neither EGDMA nor HDDMA, being the cross-linker in the HEMA solvent, had an effect on melting temperatures of embedded PEO crystals. Obviously, the polarity of the methacrylate monomer solution determines the demixing properties of PEO/methacrylate solutions.

Table 3 represents the results of screening experiments on mixtures in which the matrix monomer HEMA was partially replaced by *n*-dodecyl methacrylate (DMA). The quenching temperature was $T_Q = 123$ K, while for polymerization a temperature of $T_P = 223$ K was selected. The DSC endotherms either had one single narrow peak or showed an overlap of two peaks centered around 40 or 50 °C. Only for few endotherms, the two peaks could be clearly distinguished. Table 3 starts with a sample (Table 3, sample 22) that is reproducing results of ref 6, i.e., a monomodal peak with an onset temperature of $\vartheta_{ons} = 39.8$ °C corresponding to a tube diameter of 11.6 nm. As the amount of DMA in the matrixis increased, peaks gradually shift to higher temperatures. However, no clear indication of a shift of endotherms according to the amount of DMA in the matrix can be discerned. An overlap of at least two peaks is obtained for different samples (Table 3, samples 24−27, 29), but a separate analysis of the peaks could not be performed.

As the content of DMA in the mixture is increased, the total measured melting enthalpy remained nearly constant around 60% of the total enthalpy expected for these crystals. A further increase of DMA in the mixture could not be obtained because demixing of the monomer solution occurred even at such elevated temperatures as 80 °C.

Visualization of PEO Strands with the Aid of TEM. Semi-IPNs consisting of 20 wt % PEO-10 000 in P[(HEMA/DMA)$_{0.8}$-*cross*-HDDMA$_{0.2}$] with varying DMA contents were investigated using transmission electron microscopy. Figure 1 shows the morphology of a semi-IPN consisting of 20 wt % PEO-10000 confined to cross-linked matrix polymers made of monomers of HEMA only, i.e., 0 wt % of DMA in matrix monomers.

The PEO is obviously concentrated in cylindric wormlike strands contrasted in white with black shadows on a fracture surface otherwise homogeneously covered

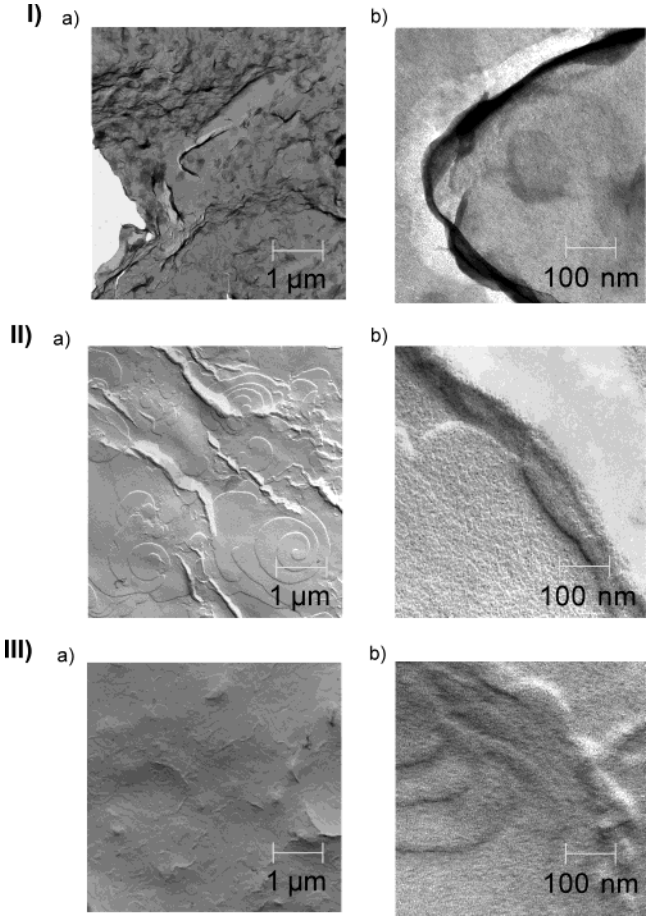

Figure 3. Replica electron micrographs of PEO nanostrands embedded in P[(HEMA/DMA)$_{0.8}$-*cross*-HDDMA$_{0.2}$] with three different DMA contents: (**I**) HEMA:DMA = 66:34; (**II**) HEMA:DMA = 50:50; (**III**) HEMA:DMA = 40:60, in two different magnifications, (a) V = 10 000 and (b) V = 100 000. The variation of the strand diameter with the DMA content is obvious although the contrast between PEO strands and matrix fades a bit with increasing diameter.

with platinum (gray color). Note that only those strands are visible that happen to lie in the fracture plane. In other terms, the cracks produced in the course of the fracture process always follow the path of lowest mechanical stability and tend, therefore, to propagate along the phase boundaries between the matrix and the PEO regions. To corroborate the true nature of the PEO strands, comparative replica pictures of the pure matrix material without PEO were acquired for different DMA contents. In these cases, no strand contrasts showed up at all.

Figure 3 shows TEM pictures of samples where the HEMA monomers were partially replaced by the less polar DMA prior to semi-IPN preparation. Strandlike structures appear again. It is demonstrated that the diameter increases with growing DMA content. Two magnifications are shown. Upon further magnification, the metal grains sputtered on the surface during film preparation can already be resolved.

Visualization of PEO Strands with the Aid of SEM. Surfaces of fractured semi-IPNs of 20 wt % PEO-10 000 in P[(HEMA/DMA)$_{0.8}$-*cross*-HDDMA$_{0.2}$] were also investigated with another electron microscopy technique, namely field-emission scanning electron microscopy (FE-SEM). Two samples were chosen with 0 and 60 wt % DMA. Figure 4 shows the corresponding micrographs for three different magnifications, 5000, 25 000, and 50 000. PEO strands are again visible, especially at the higher magnifications. Furthermore, the strand diameter is larger for the DMA containing sample in accordance to the TEM pictures.

Quantitative Evaluation of the Strand Diameter with the Aid of NMR Diffusometry. An intuitive diffusion mechanism of polymer chains confined in tube-forming pores is reptation. Since the corresponding model theory leads to echo attenuation functions depending on the tube diameter (see Appendix), NMR diffusometry permits a quantitative determination of this parameter.

Figure 5 shows typical spin−echo attenuation curves recorded in a sample consisting of 40% PEO 11200 in a methacrylate matrix of 100% HEMA, 0% DMA. The nonexponential decays as a signature of anomalous diffusion behavior are obvious. Fits of eq 19 lead to tube diameters $d_s = 9 \pm 1$ nm practically independent of the diffusion time τ_2. In this case, the "narrow-pore formula", eq 4 yields the same values, and the theoretical echo attenuation curves virtually coincide with those calculated on the basis of eq 19.

The strand diameter found for the 40% PEO sample is almost the same as that reported in ref 11 for 20 wt % PEO in the same matrix. The conclusion is that a higher percentage of PEO leads to more, but not thicker, strands.

On the other hand, changing the polarity of the initial solvent by adding DMA produces thicker strands, so that the strand diameter can be controlled by the DMA content to some degree. A series of different semi-IPNs of 20 wt % poly(ethylene oxide), M_w = 10 000, and different DMA contents was therefore prepared and examined with NMR diffusometry. Typical data sets are shown in Figure 6. Fits of eq 19 to the experimental data lead to pore diameters depending on the DMA content but practically not on the diffusion time τ_2. The average pore diameters are listed in Table 4 and plotted in Figure 7 as a function of the DMA content.

If the "narrow-pore" formula, eq 4 is fitted to the same data sets, the tube diameters for large DMA contents are found to be somewhat thicker (see Table 4), and the attenuation curves are less well described (see the dotted lines in Figure 6). This is one more indication that the diameter of the PEO strands is varying indeed, and that the reptation formalism applies under the conditions of our experiments.

Conclusions

Polymeric nanostrands in a cross-linked quasi-solid methacrylate matrix have been prepared by a spinodal demixing technique. Above the melting temperature of the confined polymer strands, diffusion can be described by reptation along the strand contour line and ordinary diffusion based on the Rouse model in lateral directions. A formalism linking field-gradient NMR diffusometry data with the strand diameter was developed. Fitting this formalism to the experimental echo attenuation data, diameters of PEO melt strands were determined in the range from 8 to 58 nm.

The demixing temperature of a PEO/methacrylate solution turned out to be of paramount importance for the characteristic length of the resulting semi-IPN's morphology. It was shown that this parameter is mainly determined by the polarity of the solvent. Hence pore diameters can be adjusted by proper selection of the matrix-forming monomer mixture to some degree.

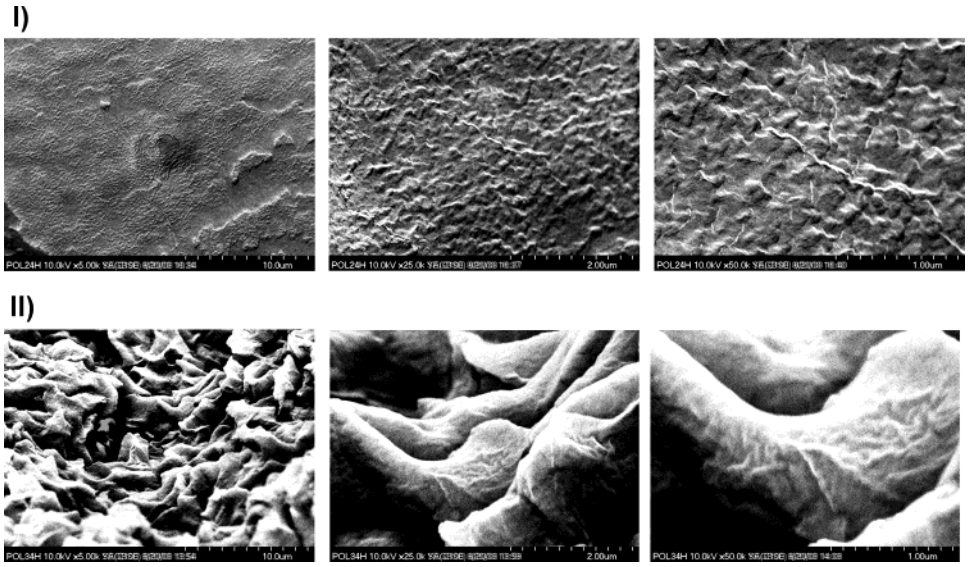

Figure 4. FE-SEM micrographs of shadow-casted surfaces of freeze-fractured semi-IPN 20% PEO-10 000 in P[(HEMA/DMA)$_{0.8}$-*cross*-HDDMA$_{0.2}$]: (**I**) HEMA:DMA = 100:0; (**II**) HEMA:DMA = 40:60. The magnifications from left to right are 5000, 25 000 and 50 000.

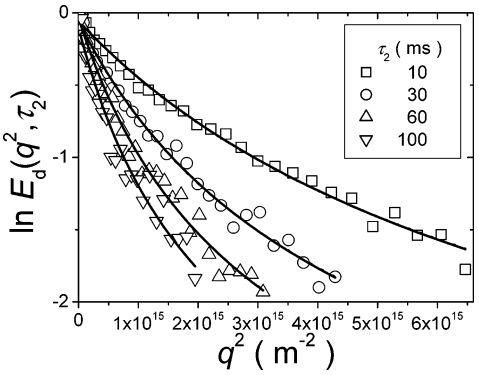

Figure 5. Typical echo attenuation curves for 40 wt % poly(ethylene oxide), M_w = 11 200, confined to pores in a methacrylate matrix (100% HEMA, 0% DMA) at 80 °C as a function of $q^2 = \gamma^2G^2\tau_1^2$ for different diffusion times τ_2. The solid lines represent fits of eq 19 (in logarithmic form) to the experimental data. The pore diameter as the only fitting parameter is found to be $d_s = 9 \pm 1$ nm for all diffusion times τ_2. In this case, fits based on the "narrow-tube formula", eq 4, lead to identical values and the theoretical attenuation curves practically coincide.

Acknowledgment. We acknowledge assistance with sample preparations by Magdalene Zimmermann. Prof. P. Walther and E. Schmid from the Electron Microscopy Centre at the University of Ulm recorded the electron micrographs. Grants from the Deutsche Forschungsgemeinschaft, the Volkswagen-Stiftung, RFBR, and CRDF are gratefully acknowledged.

Appendix: Spin−Echo Attenuation by Reptation in Wide Tubes

For diffusion times long relative to the encoding-gradient intervals, the echo attenuation function by diffusion can be written in general form as an ensemble average[10,15,16]

$$E(q,t) = \langle \exp\{iqz(t)\} \rangle \tag{3}$$

where the (spatially constant) field gradient is assumed to be directed along the z axis of the laboratory frame. Displacement components along this direction in a diffusion time t are represented by $z(t)$, and the "wavenumber" is represented by $q = \gamma G\tau_1$, where γ is the gyromagnetic ratio, G the gradient strength, and τ_1 the length of the encoding gradient interval. In a pulsed-gradient diffusometry experiment[10] τ_1 is given by the gradient pulse width δ, i.e., $\tau_1 \equiv \delta$. In a stimulated-echo experiment in the presence of steady gradients, τ_1 represents the spacing of the first two radio frequency pulses.

The angle brackets in eq 3 indicate that the ensemble average is formed with the aid of the probability density for displacements $z(t)$. At this stage no assumption concerning a Gaussian or non-Gaussian character of this probability density is yet made.

"Reptation" means that polymer chains are diffusing under topological constraints which are usually represented by a randomly coiled "tube" of diameter a. If reptation is the only translational degree of freedom of the polymers, that is, if the randomly coiled "tube" in which the diffusing polymer is confined is so narrow that all lateral displacements can be neglected, the spin−echo amplitude E as a function of the wavenumber q and the diffusion t is attenuated according to[14,15]

$$E(q,t) = \exp\left\{\frac{q^4a^2\langle s^2(t)\rangle}{72}\right\}\mathrm{erfc}\left\{\frac{q^2a\sqrt{\langle s^2(t)\rangle}}{6\sqrt{2}}\right\} \tag{4}$$

where

$$\langle s^2(t)\rangle = \frac{2D_0t}{N + \dfrac{12a^2D_0t}{N^2b^4}} + \frac{2b\sqrt{D_0t}}{\sqrt{3\pi} + 18\dfrac{\sqrt{D_0t}}{Nb}} \tag{5}$$

represents the mean squared curvilinear segment displacement in the Doi/Edwards limits $(II)_{DE}$ and $(III)_{DE}$ (for a review see ref 16). The quantities N, D_0, and b are the number of Kuhn segments per chain, the Kuhn segmental diffusivity, and the Kuhn segment length, respectively.

In context with the present study, the "tube" consists of polymer strands confined to pores of a solid matrix. That is, the polymer-filled matrix pores act as the topological constraints restricting translational diffu-

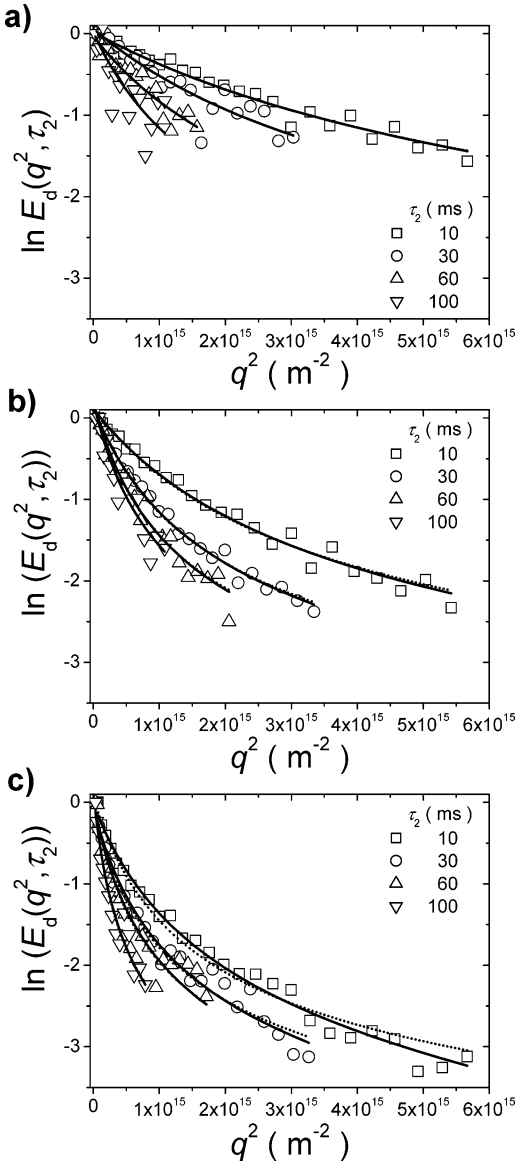

Figure 6. Typical echo attenuation curves of 20% (per weight) poly(ethylene oxide), M_w = 10 000, confined to methacrylate matrices of different composition: (a) 100 wt % HEMA, 0 wt % DMA; (b) 66 wt % HEMA, 34 wt % DMA; (c) 40 wt % HEMA, 60 wt % DMA. The data are plotted as a function of $q^2 = \gamma^2 G^2 \tau_1^2$ for different diffusion times τ_2 as indicated. The sample temperature was 80 °C in all cases. The solid lines represent fits of eq 19 (in logarithmic form) to the experimental data. The strand diameters as the only fitting parameter were found to be (a) $d_s = 8 \pm 3$ nm, (b) $d_s = 21 \pm 3$ nm, and (c) $d_s = 34 \pm 6$ nm ,practically independent of τ_2. The dotted lines represent fits of the "narrow-pore formula", eq 4, to the data.

sion. The "tube" diameter is therefore identified with the strand diameter,

$$a \equiv d_s \tag{6}$$

Since the strand diameter may be large enough to allow for perceptible displacements lateral to the contour line of the strands, the attenuation function given at eq 4 must be generalized.

The total displacement of a segment in a time t, $\delta\vec{r}(t)$, can be decomposed in components along the contour line, $\delta\vec{r}_{||}(t)$, and in lateral direction, $\delta\vec{r}_{\perp}(t)$,

$$\delta\vec{r}(t) = \delta\vec{r}_{||}(t) + \delta\vec{r}_{\perp}(t) \tag{7}$$

Table 4. Average Pore Diameters Obtained from Fits of Eq 19 and Its "Narrow-Pore" Counterpart Eq 4 to Echo Attenuation Curves of Our NMR Diffusometry Experiments[a]

id	HEMA:DMA [%: %]	fit of eq 19 d_s [nm]	fit of eq 4 d_s [nm]
22	100:0	8 ± 1	8 ± 1
23	90:10	13 ± 3	13 ± 3
24	90:10	13 ± 2	14 ± 4
25	80:20	16 ± 4	16 ± 4
26	66:34	20 ± 4	21 ± 5
27	58:42	25 ± 4	25 ± 4
28	52:48	20 ± 3	21 ± 3
29	50:50	41 ± 7	44 ± 8
30	45:55	27 ± 3	29 ± 4
31	41:59	58 ± 6	60 ± 10
32	40:60	31 ± 4	34 ± 5
33	40:60	34 ± 6	40 ± 8

[a] d_s: averaged fitted strand diameter for diffusion times τ_2 = 10, 15, 20,30,40, 60, 100, and 150 ms.

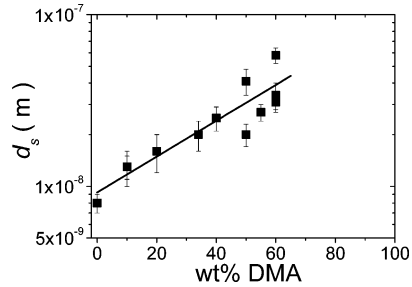

Figure 7. Fitted strand diameters for 20% (per weight) poly(ethylene oxide), M_w = 10 000, confined to P[(HEMA/DMA)$_{0.8}$-*cross*-HDDMA$_{0.2}$] as a function of the ratio(per weight) of DMA compared to HEMA prior to matrix preparation (see Table 4, samples 22−33). The diameter data are averages over 10 different τ_2 intervals ranging from 10 to 100 ms. The straight line represents an exponential function.

This is illustrated in Figure 8, where the translational displacement of a representative segment along the contour line inside a pore is shown. The corresponding relation for the mean squared displacements reads

$$\langle \delta r^2 \rangle = \langle \delta r_{||}^2 \rangle + \langle \delta r_{\perp}^2 \rangle \tag{8}$$

where any correlation between $\delta\vec{r}_{||}(t)$ and $\delta\vec{r}_{\perp}(t)$ has been neglected.

The general expression for the spin−echo attenuation given at eq 3 thus becomes

$$E(q,t) = E_{||}(q,t)E_{\perp}(q,t) = \langle e^{i\vec{q}\cdot\vec{r}_{||}(t)} \rangle \langle e^{i\vec{q}\cdot\vec{r}_{\perp}(t)} \rangle \tag{9}$$

The factor $E_{||}(q,t) \equiv \langle e^{i\vec{q}\cdot\vec{r}_{||}(t)} \rangle$ coincides with the expression given at eq 4 for reptation in a thin tube.[14] The second factor, $E_{\perp}(q,t) \equiv \langle e^{i\vec{q}\cdot\vec{r}_{\perp}(t)} \rangle$, describes the additional spin−echo attenuation due to the finite thickness of the confined strands, i.e., the displacements in directions lateral to the contour line. Assuming for simplicity a Gaussian probability distribution for $\delta\vec{r}_{\perp}(t)$ leads to

$$E_{\perp}(q,t) = e^{-q^2 \langle \delta r_{\perp}^2(t) \rangle / 6} \tag{10}$$

Let us now estimate $\langle (\delta\vec{r}_{\perp}(t))^2 \rangle$. For short times, when $\langle (\delta\vec{r}_{\perp}(t))^2 \rangle \ll d_s^2$, the motion of the polymer segments is free and can be described by Rouse dynamics.[4] In this limit, we have therefore

$$\langle (\delta\vec{r}_{\perp}(t))^2 \rangle \approx \frac{2}{3} \langle (\delta\vec{r}(t))^2 \rangle_R \ll d_s^2 \tag{11}$$

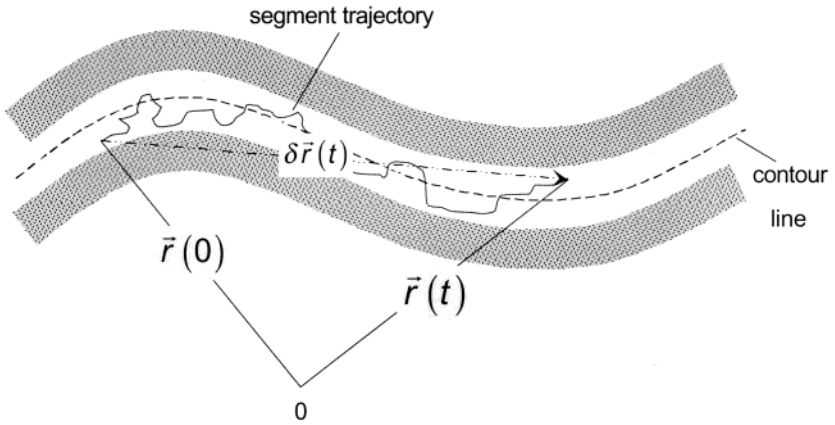

Figure 8. Schematic illustration of a segment trajectory in a pore in a time t. The total displacement $\delta\vec{r}(t)$ can be decomposed to a curvilinear displacement along the contour line of the pore and a displacement perpendicular to the contour line.

where $\langle(\delta\vec{r}(t))^2\rangle_R$ is the mean squared displacement predicted by the Rouse model. The factor $^2/_3$ takes into account that displacements are considered only in a plane perpendicular to the contour line of the strand. In the opposite limit, $\langle(\delta\vec{r}_\perp(t))^2\rangle \gg d_s^2$, i.e., when the displacements in free space would be much larger than the strand diameter, the lateral mean squared displacement $\langle(\delta\vec{r}_\perp(t))^2\rangle$ no longer depends on the time. The segment can be located at any position in the transverse plane, so that we find after some elementary calculations for this limit

$$\langle(\delta\vec{r}_\perp(t))^2\rangle = \left(\frac{d_s}{2}\right)^2 \tag{12}$$

where we have assumed a circular shape of the strand cross-section.

Using the asymptotically exact results of eq 11 (short-time limit) and eq 12 (long-time limit), we find the following interpolation expression for all times:

$$\langle(\delta\vec{r}_\perp(t))^2\rangle = \frac{\frac{2}{3}\langle\vec{r}^{\,2}(t)\rangle_R}{1+\frac{8}{3}\frac{\langle\vec{r}^{\,2}(t)\rangle_R}{d_s^{\,2}}} \tag{13}$$

In the limit $t > \tau_R$, we have for the mean squared segment displacement according to the Rouse model

$$\langle\vec{r}^{\,2}(t)\rangle_R = 6\frac{D_0}{N}t \tag{14}$$

and for the mean squared curvilinear segment displacement along the contour line[14,16]

$$\langle s^2(t)\rangle = 2\frac{D_0}{N}t \tag{15}$$

that is

$$\langle\vec{r}^{\,2}(t)\rangle_R = 3\langle s^2(t)\rangle \tag{16}$$

where $D_0 = (k_BT/\zeta)$ is the segmental diffusion coefficient, ζ is the segmental friction coefficient, and k_BT is the Boltzmann constant times the absolute temperature. Taking all factors together, the echo attenuation factor for displacements perpendicular to the contour line reads

$$E_\perp(q,t) = \exp\left\{-\frac{1}{6}q^2\langle\delta r_\perp^{\,2}(t)\rangle\right\} = \exp\left\{-\frac{1}{6}q^2\frac{\frac{2}{3}\langle\vec{r}^{\,2}(t)\rangle_R}{1+\frac{8}{3}\frac{\langle\vec{r}^{\,2}(t)\rangle_R}{d_s^{\,2}}}\right\} = \exp\left\{-\frac{1}{6}q^2\frac{2\langle s^2(t)\rangle}{1+8\frac{\langle s^2(t)\rangle}{d_s^{\,2}}}\right\} \tag{17}$$

Combining this with Eqs 9 and 4 leads to the total echo attenuation function

$$E(q,t) = E_{||}(q,t)E_\perp(q,t) = \exp\left\{\frac{q^4 d_s^{\,2}\langle s^2(t)\rangle}{72}\right\} \times \operatorname{erfc}\left\{\frac{q^2 d_s\langle s^2(t)\rangle}{6\sqrt{2}}\right\} \exp\left\{-\frac{1}{6}q^2\frac{2\langle s^2(t)\rangle}{1+2\langle s^2(t)\rangle\left(\frac{2}{d_s}\right)^2}\right\} \tag{18}$$

with an additional exponential factor for displacements perpendicular to the strand contour line.

For times longer than the Rouse relaxation time, $t > \tau_R$, that is for the Doi/Edwards limit $(III)_{DE}$, the mean-squared curvilinear segment displacement is predicted to obey eq 15, which is expected to provide the dominating contribution to spin−echo attenuation by reptation under the usual experimental conditions. The mean-squared curvilinear segment displacement given at eq 5 can be approximated by eq 15 Evaluations of echo attenuation curves on this basis coincided with those obtained using the full expression given at eq 5 for limits $(II)_{DE}$ and $(III)_{DE}$ together. The final evaluation formula used in this study thus reads

$$E(q,t) = \exp\left\{\frac{q^4 d_s^{\,2} D_0 t}{36N}\right\}\operatorname{erfc}\left\{\frac{q^2 d_s\sqrt{D_0 t}}{6\sqrt{N}}\right\} \times \exp\left\{-\frac{\frac{2}{3}q^2 D_0 t}{N+4D_0 t\left(\frac{2}{d_s}\right)^2}\right\} \tag{19}$$

Quantitative values of the parameters can be estimated

using literature data[17,18] for bulk PEO melts assuming that these parameters are not affected by pore confinements: $N = M_w/85.3$, $D_0 = 9.66 \times 10^{-10}$m/s^2, and $b = 8.38 \times 10^{-10}$m. The only parameter remaining to be fitted to experimental data thus is the strand diameter d_s (apart from a normalization constant).

References and Notes

(1) Millar, J. R. *J. Chem Soc.* **1960**, 1311.
(2) Sperling, L. H. *Interpenetrating networks and related materials*; Plenum Press: New York, 1981.
(3) de Graaf, L.; Albers, P−J. W.; Möller, M. *J. Polym. Sci., Part B: Polym. Phys.* **1996**, *34*, 1893.
(4) Doi, M.; Edwards, S. F. *The Theory of Polymer Dynamics*; Clarendon Press: Oxford, England, 1986.
(5) Mattea, C.; Fatkullin, N.; Fischer, E.; Beginn, U.; Anoardo, E.; Kroutieva, M.; Kimmich, R. *Appl. Magn. Reson.*, in press.
(6) Beginn, U.; Fischer, E.; Pieper, T.; Mellinger, F.; Kimmich, R.; Möller, M. *J. Polym. Sci., Part A: Polym. Chem.* **2000**, *38*, 2041.
(7) Cahn, J. W. *J. Chem. Phys.* **1965**, *42*, 93.
(8) Smolders, C. A.; van Aartsen, J. J.; Steenberg, A. *Kolloid Z. Z. Polym.* **1971**, *243*, 14.
(9) Hiemenz, P. C.; *Polymer Chemistry−The Basic Concepts*, 2nd ed.; Marcel Dekker: New York, 1984l; p 214.
(10) Ardelean, I.; Kimmich, R. *Annu. Rep. NMR Spectrosc.* **2003**, *49*, 43.
(11) Fischer, E.; Kimmich, R.; Beginn, U.; Möller, M. *Phys. Rev. E.* **1999**, *59*, 4079.
(12) Fischer, E.; Kimmich, R. *J. Magn. Reson.* **2004**, *166*, 273.
(13) de Gennes, P. G. *J. Chem. Phys.* **1971**, *55*, 572.
(14) Fatkullin, N.; Kimmich, R. *Phys. Rev. E* **1995**, *52*, 3273.
(15) Kimmich, R. *NMR tomography, diffusometry, relaxometry*, Springer-Verlag: Berlin, 1997.
(16) Kimmich, R.; Fatkullin, N. *Adv. Polym. Sci.* **2004**, *170*.
(17) Graessley, W. W.; Edwards, S. F. *Polymer* **1981**, *22*, 1329.
(18) Smith, G. D.; Yoon, D. Y.; Jaffe, R. L.; Colby, R. H.; Krishnamorti, R.; Fetters, L. J. *Macromolecules* **1996**, *29*, 3462.

MA0358226